Available online at www.sciencedirect.com
ScienceDirect
Geochimica et Cosmochimica Acta 70 (2006) 5723–5739
Geochimica
www.elsevier.com/locate/gca

Evolution of the oceanic sulfur cycle at the end of the Paleoproterozoic

David T. Johnston [a,*], Simon W. Poulton [b], Philip W. Fralick [c], Boswell A. Wing [a,d], Donald E. Canfield [e], James Farquhar [a,f]

[a] Department of Geology and ESSIC, University of Maryland, College Park, MD 20742, USA
[b] School of Civil Engineering and Geosciences, University of Newcastle upon Tyne, NE1 7RU, UK
[c] Department of Geology, Lakehead University, Thunder Bay, Ont., Canada
[d] Department of Earth and Planetary Sciences, McGill University, Montreal, Que., Canada
[e] Nordic Center for Earth Evolution and Institute of Biology, University of Southern Denmark, Campusvej 55, 5230 Odense M, Denmark
[f] Hanse Wissenschaftskolleg, Lehmkuhlenbusch 4, 27753 Delmenhorst, Germany

Received 11 May 2006; accepted in revised form 2 August 2006

Abstract

Here, we present new measurements of ^{32}S, ^{33}S, ^{34}S, and ^{36}S in sedimentary sulfides and couple these measurements with modeling treatments to study the sulfur cycle of a late Paleoproterozoic marine basin. We target the transition in ocean chemistry from the deposition of Paleoproterozoic iron formations (Gunflint Formation, Biwabik Formation, Trommald Formation, and Mahnomen iron formations) to the inferred sulfidic ocean conditions recorded by overlying shale (Rove Formation). The data suggest that certain features of the global sulfur cycle, such as a control by sulfate reducing prokaryotes, and low (mM) concentrations of oceanic sulfate, were maintained across this transition. This suggests that the transition was associated with changes in the structure of the basin-scale sulfur cycle during deposition of these sediments. Sulfide data from the iron formations are interpreted to reflect sedimentary sulfides formed from microbial reduction of pore-water sulfate that was supplied through steady-state exchange with an overlying oceanic sulfate reservoir. The sulfide data for the euxinic Rove Formation shales reflect the operation of a sulfur cycle that included the loss of sulfide by a Rayleigh-like process. We suggest that the prevalence of large and variable heavy isotope enrichments observed in Rove Formation sulfide minerals reflect a sustained and significant net loss of sulfide from the euxinic water column, either as a result of a shallow chemocline and degassing to the atmosphere or as a result of a water column pyrite sink. The inclusion of ^{36}S measurements (in addition to ^{32}S, ^{33}S, and ^{34}S) illustrates the mass-dependent character of these sedimentary environments, ruling out contributions from the weathering of Archean sulfides and pointing to at least modest levels of sustained atmospheric oxygen ($>10^{-5}$ present atmospheric levels of O_2).

1. Introduction

Recent studies of redox sensitive elements, mineral speciation, and isotopic systems have indicated a transition from ferruginous (Fe^{2+}-rich) to widespread euxinic (S^{2-}-rich) water-column conditions coincident with the cessation of iron formation (IF) deposition in the late Paleoproterozoic (Poulton et al., 2004). Sulfidic conditions are thought to have become widespread at the time of this transition, persisted into the middle Proterozoic, and may have had profound effects on the isotopic composition and size of the seawater sulfate reservoir (Canfield, 1998; Shen et al., 2002, 2003; Arnold et al., 2004; Canfield, 2004; Rouxel et al., 2005). The lithologic progression from iron formation (Gunflint Formation, Biwabik Formation, Trommald Formation, and the Mahnomen Formation) to shale (Rove Formation) in the Animike Basin, North America, has been interpreted as capturing the transition from ferruginous to sulfidic conditions (Poulton et al., 2004). The observation of a high proportion of highly reactive iron (Fe_{HR}) to total iron (Fe_{Total})($Fe_{HR}/Fe_{Total} > 0.38$)

* Corresponding author. Fax: +1 301 405 8611.
E-mail address: dtj@geol.umd.edu (D.T. Johnston).

0016-7037/$ - see front matter © 2006 Elsevier Inc. All rights reserved.
doi:10.1016/j.gca.2006.08.001

points to persistent anoxic bottom water conditions throughout this succession, and the ratio of pyrite iron (Fe_{Py}) to highly reactive iron indicates a change from ferruginous conditions during deposition of the Gunflint Formation ($Fe_{Py}/Fe_{HR} = 0.001 \pm 0.001$) to sulfidic conditions in the upper Rove Formation ($Fe_{Py}/Fe_{HR} = 0.87 \pm 0.04$). In this study, we evaluate 38 new measurements of the four stable sulfur isotopes (^{32}S, ^{33}S, ^{34}S, and ^{36}S) for Cr-reducible sulfur (herein referred to as sulfide) from samples of the laterally equivalent Gunflint Iron Formation ($n = 10$), Biwabik Iron Formation ($n = 3$), Trommald Iron Formation ($n = 5$), and Mahnomen Formation ($n = 3$), with additional samples from the overlying Rove Formation ($n = 17$) (Table 1). Our approach expands on that used in prior studies of sulfur isotopes because it includes new modeling and evaluates the significance of $\delta^{33}S$ and $\delta^{36}S$ in addition to the more commonly reported $\delta^{34}S$.

2. Setting, systems, and methods

2.1. Geologic setting

At approximately 2450 Ma, a rift to passive margin developed along the southern edge of Superior Province when a land-mass to the south separated (Fralick and Miall, 1989). Later closure of the resultant ocean led to the deposition of the Animikie and North Range Groups as a backarc basin developed (Hemming et al., 1995; Van Wyck and Johnson, 1997; Pufahl et al., 2000; Poulton and Canfield, 2005), which, with a collision, was later

Table 1
All sulfur isotope data grouped (*WC* [water column], *Formation*, and *sample*) according to Poulton et al. (2004)

WC	Formation	Sample	$\delta^{34}S^*$	$\delta^{34}S$	$\Delta^{33}S$	$\Delta^{36}S$
Sulfidic	Rove Fm.	R40	17.99	17.84	−0.027	0.48
Sulfidic	Rove Fm.	R38	23.9	25.19	0.006	0.25
Sulfidic	Rove Fm.	R35	21.45	23.02	−0.031	0.33
Sulfidic	Rove Fm.	R34	17.27	17.98	0.054	0.27
Sulfidic	Rove Fm.	R33	10.75	11.67	0.041	0.02
Sulfidic	Rove Fm.	R32	16.34	17.42	−0.047	0.64
Sulfidic	Rove Fm.	R31	20.98	22.43	−0.019	0.46
Sulfidic	Rove Fm.	R30	13.44	4.95	0.038	0.02
Sulfidic	Rove Fm.	R29	9.42	9.28	0.078	−0.29
Transitional	Rove Fm.	R28	14.9	18.06	0.002	0.38
Transitional	Rove Fm.	R27	12	12.00	−0.008	0.13
Transitional	Rove Fm.	R26g	9.97	9.99	−0.015	0.58
Transitional	Rove Fm.	R24	5.13	4.15	−0.013	0.26
Transitional	Rove Fm.	R15b	31.88	32.92	0.031	0.21
Transitional	Rove Fm.	R15a	21.54	22.93	0.036	0.34
Transitional	Rove Fm.	T35	5.9	6.18	−0.015	0.55
Transitional	Rove Fm.	T29	−1.17	−0.96	0.018	0.11
Silicified	*Gunflint Fm.*	*T26*	*3.45*	*3.82*	*0.002*	*0.08*
Silicified	*Gunflint Fm.*	*T25*	*1.97*	*1.47*	*0.049*	*−0.35*
Silicified	*Gunflint Fm.*	*R5*	*21.33*	*13.75*	*0.003*	*0.17*
Silicified	*Gunflint Fm.*	*T24*	*21.78*	*21.96*	*0.012*	*0.24*
Ferruginous	Gunflint Fm.	T19	9.95	10.20	−0.034	0.51
Ferruginous	Gunflint Fm.	R2	9.41	10.22	−0.009	0.57
Ferruginous	Gunflint Fm.	T13	12.18	13.33	−0.046	0.76
Ferruginous	Gunflint Fm.	S22	1.44	−0.50	−0.028	0.45
Ferruginous	Gunflint Fm.	S21	−1.18	−0.43	−0.003	0.26
Ferruginous	Gunflint Fm.	S1	4.75	4.07	−0.008	0.32
Ferruginous	Biwabik Fm.	B44	—	6.97	−0.032	0.19
Ferruginous	Biwabik Fm.	B26	—	9.83	−0.056	0.44
Ferruginous	Biwabik Fm.	B3	—	3.26	0.003	0.27
Ferruginous	Trommald Fm.	M13	11.35	12.24	−0.051	0.49
Ferruginous	Trommald Fm.	M16	14.66	15.53	−0.073	0.70
Ferruginous	Trommald Fm.	M24	6.66	7.73	−0.048	0.54
Ferruginous	Trommald Fm.	M25	7.92	8.05	−0.027	0.73
Ferruginous	Trommald Fm.	M27	8.33	8.65	−0.051	0.70
Ferruginous	Mahnomen Fm.	M30	9.64	9.71	−0.062	0.51
Ferruginous	Mahnomen Fm.	M31	8.31	9.59	−0.052	1.03
Ferruginous	Mahnomen Fm.	M37	12.54	13.58	−0.051	0.76

Samples from the Gunflint and Rove Fms. are arranged in stratigraphic order. Values labeled $\delta^{34}S^*$ are taken from Poulton et al. (2004) and represent sulfur isotope abundance measurements using the SO_2 technique. Samples labeled as silicified (italics) have been visually identified as compromised by secondary processes. These measurements are included in this table and Section 3, but not interpreted as representative of the depositional environments. Transitional samples have been selected on the basis of Fe-speciation methods (Poulton and Canfield, 2005). Values for $\Delta^{3x}S$ have been calculated according to Eqs. (2) and (3). Uncertainties are estimated at 0.12, 0.008, and 0.20 (1σ) for $\delta^{34}S$, $\Delta^{33}S$, and $\Delta^{36}S$.

transformed into a foreland setting (Hoffman, 1987; Southwick and Morey, 1991; Hemming et al., 1995; Ojakangas et al., 2001; Maric and Fralick, 2005). Initial south to north flooding of the backarc led to deposition of siliciclastic tidal deposits (Ojakangas, 1983) forming the Mahnomen, Pokegama, and Kakabeka Formations (Fig. 1). These are

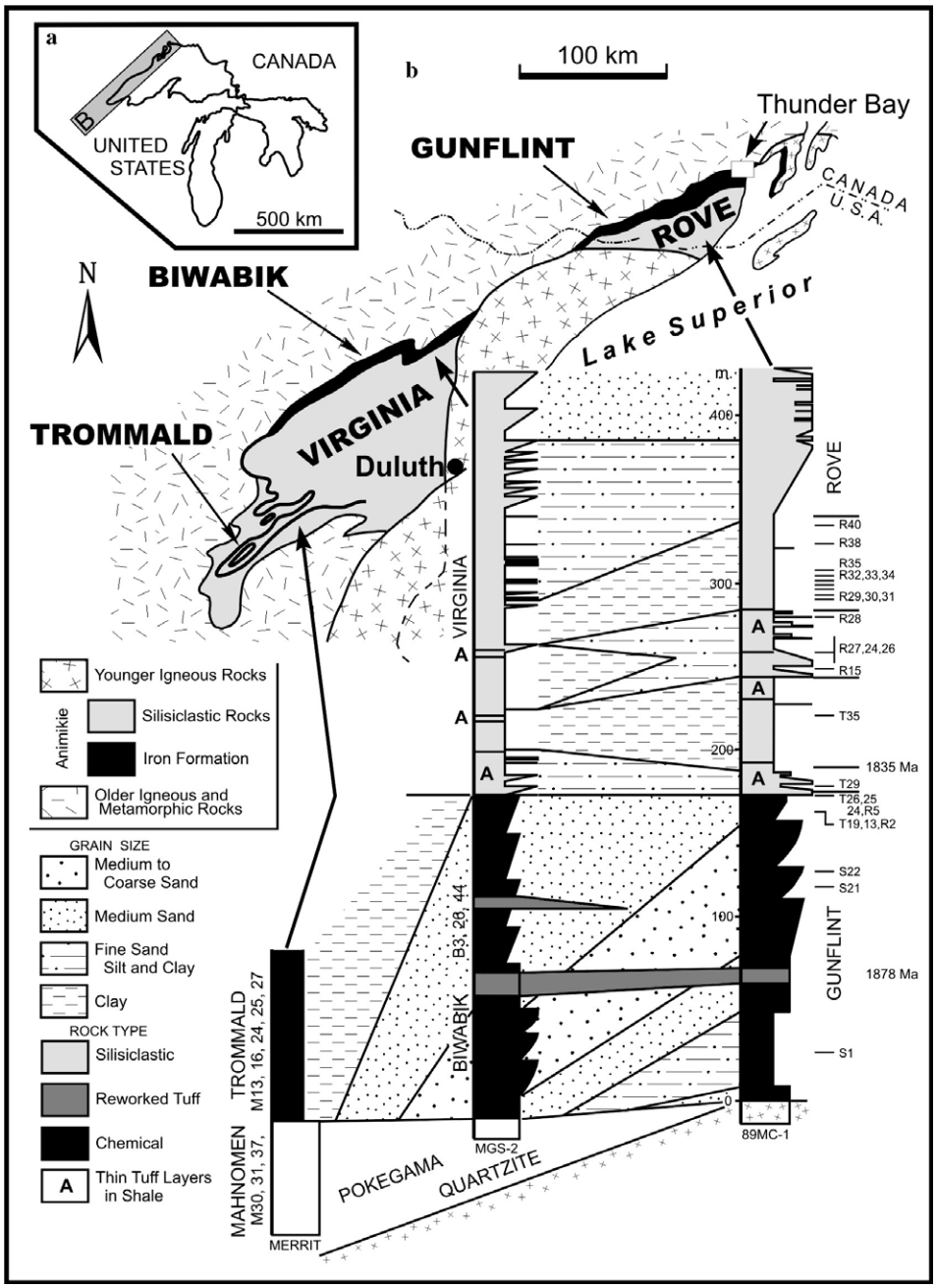

Fig. 1. Geology and location of the Animikie Basin (a) Location map. (b) Animikie sedimentary rocks generally dip gently to the southeast with their lower unconformable contact with Neoarchean rocks exposed to the northwest. The southernmost portion of the basin is more intensely deformed, and there structural contacts are probably present. Mesoproterozoic intrusive rocks related to the Mid-Continental Rift divide the basin and Rift basalts overlie the basin. The stratigraphic sections depict the rocks present in three continuously cored drill-holes. Shales to sandstones of the Mahnomen Formation and Pokegama Quartzite underlie the Trommald, Biwabik, and Gunflint iron formations. The Trommald is dominated by fine-grained iron and manganese oxides deposited in the outer shelf to slope environment (ocean to the south, shoreline to the north) (Pufahl et al., 2000). Cycles containing fine-grained chemical sedimentary rocks overlain by coarsening-upwards grainstone assemblages, composed of chert, iron oxide and iron carbonate sand, dominate these shallow shelf deposits. Two tuff layers provide chronostratigraphic markers and show that the lithofacies boundaries are diachronous and reflect south to north transgression–regression–transgression (Fralick and Barrett, 1995; Pufahl et al., 2000). A hiatus appears to occur between the iron formation and the overlying siliciclastic rocks of the Virginia and Rove Formations (Addison et al., 2005). See the text for a more detailed discussion. Figure from data in Pufahl and Fralick (1995) and Maric and Fralick (2005). Sample positions are indicated to the right of the stratigrpahic column, with width of the column indicating grain size.

thickest in the south, forming only a sporadically developed basal conglomerate in the northernmost area. The chemical sediment dominated Trommald, Biwabik and Gunflint Formations overlie the basal siliciclastics (Fig. 1). Chemical sediments are also prominent within parts of the Mahnomen Formation. These units are primarily composed of both granular and fine-grained iron oxides, carbonates and chert. The sedimentary strata are organized into fining- and coarsening-upward successions reflecting transgressive-regressive cycles (Fralick and Barrett, 1995) on an open, wave and tide dominated shelf (Ojakangas, 1983; Fralick, 1988; Pufahl et al., 2000; Poulton and Canfield, 2005). Water depths during the deposition of these chemical sediments, even on the mid-shelf, probably did not exceed 10 s of meters (Pufahl and Fralick, 2004). U–Pb age determinations of zircons from a reworked tuff in the Gunflint Formation yielded an age of 1878+ −1 Ma (Fralick et al., 2002). Deposition of the iron formations probably ended in the northern area, and possibly to the south, as closure with a land-mass to the south caused upwarping and withdrawal of the sea (Addison et al., 2005) during the 1860–1835 Ma (Sims et al., 1989) Penokean Orogeny. During this interval, at approximately 1850 Ma (Krogh et al., 1984), a large hypervelocity impact occurred 700 km to the east, near Sudbury, and the ejecta is present very near the top of the Gunflint and Biwabik Formations (Addison et al., 2005). This uppermost portion of the Gunflint is highly altered with intense silicification and the development of agate and pyrite veins and vugs. The alteration may be the result of subareal exposure during a hiatus inferred from a U–Pb age on zircons of approximately 1835 Ma from tuffs immediately above the Gunflint and Biwabik Formations (Addison et al., 2005). These tuffs are contained in the Virginia and Rove Formations (Fig. 1). The lower 100–150 m of these units consists of alternating shale-siltstone and black, pyritiferous shale successions, probably reflecting fluctuations in sea level (Maric and Fralick, 2005). These successions, and especially the upper black shale, likely represent a major condensed interval deposited in water ~100 to 200 m deep. Lucente and Morey (1983) ascribed sedimentation of this interval to pelagic rainout of fine-grained sediment from dilute suspension or hemipelagic processes involving diffuse turbidity currents. The presence of abundant, sub-millimeter rip-up intraclasts also denotes the operation of sporadic bottom currents (Maric and Fralick, 2005). Tidal deposits present in correlative rocks to the south of Lake Superior (Ojakangas et al., 2001) confirm open connection to the ocean. Above the upper, pure black shale interval, graded fine-grained sandstones are organized into a coarsening-upward succession approximately 100 m thick that is transitional into 400 m of medium-grained, sandstone-dominated, stacked parasequences (Maric and Fralick, 2005). This is overlain by lenticular to wavy bedded sandstones and shales with both wave and current ripples. The coarsening-upward to sandstone-dominated portion of the Virginia and Rove Formations has been interpreted as a submarine fan (Lucente and Morey, 1983; Maric and Fralick, 2005) with the uppermost ripple laminated succession representing progradation of distal distributary mouth bars of a delta (Maric and Fralick, 2005). A sandstone sample from the submarine fan portion of the succession yielded a youngest U–Pb detrital zircon age of approximately 1780 Ma (Heamen et al., 2005). The predominantly Paleoproterozoic zircon population (Heamen et al., 2005), and paleocurrents indicating sediment derivation from the north (Morey, 1973), strongly suggest the Trans-Hudson Orogen was the source of the detritus. The northern sedimentary rocks of the Animikie Basin are essentially undeformed and unmetamorphosed, making them ideal targets for the study of low temperature biogeochemical cycling.

2.2. Analytical methods

The majority of the samples examined here were previously studied by Poulton et al. (2004) using methods described in Poulton and Canfield (2005). All additional samples were chemically prepared in the same manner as those previously studied (Poulton et al., 2004). In addition to the samples prepared for this study, splits of the Ag_2S extracted as Cr-reducible sulfur (considered to be pyrite; Canfield et al., 1986) by Poulton et al. (2004) were converted to SF_6 by reaction with a 10-fold excess of F_2 at 250 °C for 8 h in a Ni reaction vessel. After the reaction, product SF_6 was condensed from the residual F_2 into a liquid-nitrogen cooled trap (−177 °C), and subsequently distilled from a trap at −115 °C to the injection loop of a gas chromatograph (GC) at −177 °C. GC purification of SF_6 was undertaken using a 1/8 in. diameter, 12 foot long Haysep-Q™ column with a He carrier flow at 20 mL/min. The SF_6 peak was registered on a TCD and then isolated by freezing into a liquid-nitrogen cooled trap. The isotopic composition of the purified SF_6 was determined by dual-inlet gas-source mass spectrometry monitoring ion beams at *m/e* of 127, 128, 129, and 131 using a Thermo Finnigan MAT 253 gas source mass spectrometer.

2.3. Isotope notation

Isotopic ratios ($^{3i}R = {}^{3i}S/{}^{32}S$) are reported using standard delta notation,

$$\delta^{3i}S = \left(\frac{{}^{3i}R_{\text{sample}}}{{}^{3i}R_{\text{V-CDT}}} - 1\right) \times 1000, \tag{1}$$

where 3*i* is 33, 34, or 36. We also use capital delta notation, where

$$\Delta^{33}S = \delta^{33}S - 1000 \times \left(\left(1 + \frac{\delta^{34}S}{1000}\right)^{0.515} - 1\right), \tag{2}$$

and

$$\Delta^{36}S = \delta^{36}S - 1000 \times \left(\left(1 + \frac{\delta^{34}S}{1000}\right)^{1.90} - 1\right) \tag{3}$$

(Hulston and Thode, 1965; Farquhar et al., 2000). The data are reported relative to V-CDT assuming that IAEA S-1 reported on the VCDT scale has a $\delta^{33}S = -0.05‰$ (Gao and Thiemens, 1993; Ding et al., 2001), $\delta^{34}S = -0.30‰$ (Ding et al., 2001; Krouse and Coplen, 1997; Gao and Thiemens, 1993), and assuming a $\delta^{36}S = -1.26‰$. Uncertainties are estimated from the reproducibility of repeat analyses of IAEA standards and are 0.12‰, 0.008‰, and 0.2‰ (1σ) for $\delta^{34}S$, $\Delta^{33}S$, and $\Delta^{36}S$, respectively. Uncertainties between $\delta^{33}S$, $\delta^{36}S$, and $\delta^{34}S$ are mass-dependently correlated, resulting in $\Delta^{33}S$ and $\Delta^{36}S$ uncertainties that are smaller than for $\delta^{33}S$ and $\delta^{36}S$, respectively.

2.4. Modeling treatments

We use a box model of the surface sulfur cycle (cf., Garrels and Lerman, 1981) to evaluate how sulfur moves between different terrestrial sulfur reservoirs and to make predictions about the $\delta^{33}S$, $\delta^{34}S$, and $\delta^{36}S$ of Proterozoic seawater sulfate. A previous study used a similar approach and considered the isotopic fractionations associated with sulfate reduction and re-oxidative processes such as disproportionation (see Johnston et al., 2005a for a more detailed description). The form of the model in this study is presented in Fig. 2, and is modified from Johnston et al. (2005a) in order to account for some new features of the data (sulfides enriched in ^{34}S).

3. Results

The data are presented in Table 1. The ranges of $\delta^{34}S$, $\Delta^{33}S$, and $\Delta^{36}S$ are −0.96 to 32.92‰, −0.073 to 0.078‰, and −0.35 to 1.03‰, respectively. Our $\delta^{34}S$ data parallel those presented in Poulton et al. (2004) with the IF (lower Gunflint, Biwabik Trommald, and the underlying siliciclastic Mahnomen Formations) yielding an average $\delta^{34}S$ of $8.4 \pm 4.6‰$ (1σ), the lower ~100 m of the Rove Formation (assigned to a transitional environment between ferruginous and persistent euxinia; Poulton et al., 2004) yielding an average $\delta^{34}S$ of $13.2 \pm 11.0‰$ (1σ), and the data for the upper 'sulfidic' Rove Formation yielding an average $\delta^{34}S$ of $16.6 \pm 6.8‰$ (1σ).

Comparison of new SF_6 analyses with earlier SO_2-based analyses of the same Ag_2S precipitates suggests a correlation of $\delta^{34}S_{SF_6} = 1.009(\pm 0.051; 1\sigma)\ \delta^{34}S_{SO_2} - 0.066(\pm 0.711; 1\sigma)$. However, when three significant outliers ($>3\sigma$; R30, R28, and R5) are removed from the comparison, the same linear regression technique suggests a correlation of $\delta^{34}S_{SF_6} = 1.055(\pm 0.016; 1\sigma)\ \ \delta^{34}S_{SO_2} - 0.166(\pm 0.210; 1\sigma)$. Both predicted correlations are within 2σ of comparisons of these two methods ($\delta^{34}S_{SF_6} = 1.035\delta^{34}S_{SO_2} - 0.135$; Rees, 1978), in which the differences are interpreted to reflect scale compression on the SO_2 measurements as a result of memory effects.

Our results for ^{33}S and ^{36}S yield $\Delta^{33}S$ and $\Delta^{36}S$ of -0.037 ± 0.022 and $0.54 \pm 0.22‰$ for the IF, -0.004 ± 0.021 and $0.32 \pm 0.18‰$ for the transitional

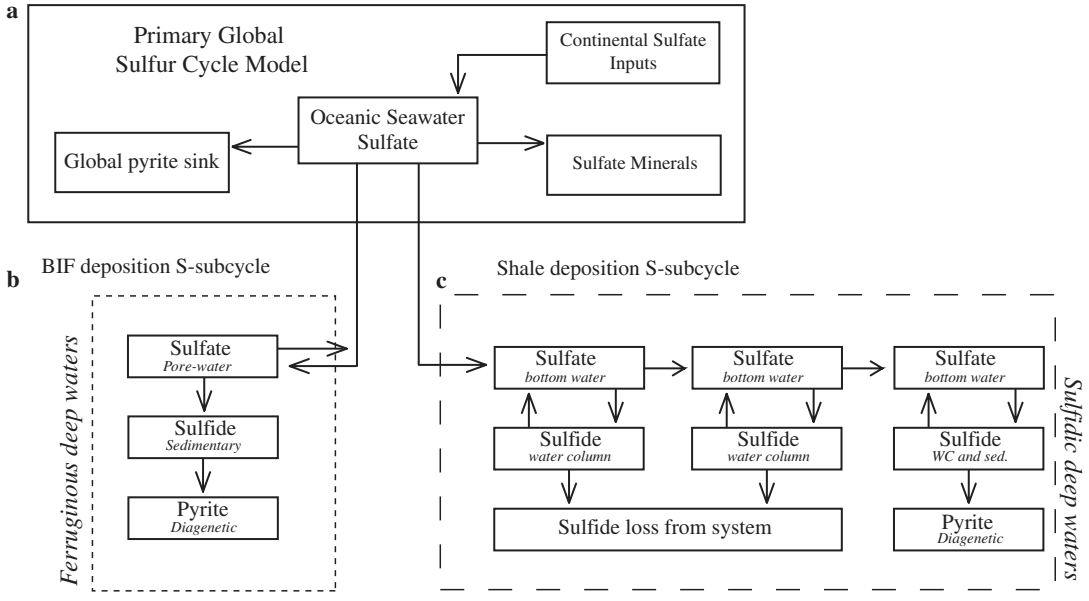

Fig. 2. A box model representation of the global steady-state sulfur cycle. Arrows represent fluxes between reservoirs (boxes). The relative placement of the boxes in the figure is independent of the actual environmental location of the pool. (a) We model a global sulfur cycle with one source (continental/riverine) and two global sinks (sulfide and sulfate minerals). The recycling of the oceanic sulfur pools (global sulfide and global sulfate minerals) is not incorporated here due to the relatively short depositional period represented by these sediments. (b) The modeled sub cycle used to describe the BIF depositional environment. Here, the global seawater sulfate reservoir feeds to a ferruginous deeper water reservoir. (c) The modeled sub cycle used to describe the shale depositional environment. In order to satisfy the data using a steady state model, multiple sulfide reservoirs were included in the sub cycle.

shales, and 0.010 ± 0.044 and $0.24 \pm 0.29‰$ for the upper euxinic Rove Formation samples. The IF data cluster towards lower $\delta^{34}S$, negative $\Delta^{33}S$, and positive $\Delta^{36}S$, whereas the shale data cover almost the entire data set. No strong stratigraphic trends are observed within the data, although a slight positive trend in $\delta^{34}S$ and $\Delta^{33}S$ (negative in $\Delta^{36}S$) is observed moving up-column. The $\Delta^{36}S$ and $\Delta^{33}S$ values are correlated and form an array given by $\Delta^{36}S = -6.28$ (± 0.78; 1σ) $\Delta^{33}S + 0.300$ (± 0.029; 1σ) (with sub-trajectories of $\Delta^{36}S = -5.58$ (± 2.12; 1σ) $\Delta^{33}S + 0.336$ (± 0.091; 1σ), $\Delta^{36}S = -3.76$ (± 3.08; 1σ) $\Delta^{33}S + 0.338$ (± 0.063; 1σ), $\Delta^{36}S = -5.77$ (± 1.12; 1σ) $\Delta^{33}S + 0.301$ (± 0.048; 1σ), and $\Delta^{36}S = -10.31$ (± 2.79; 1σ) $\Delta^{33}S + 0.201$ (± 0.064; 1σ) for the IF, transitional shale, sulfidic shale, and silicified samples, respectively).

4. Discussion

Previously published treatments of the sulfur cycle suggest that the sulfur isotope composition of the oceanic sulfate and sedimentary sulfide pools depends on material-balance constraints given by the fraction of sulfur lost to pyrite burial (f_{py}), the magnitude of fractionation by sulfate reducing bacteria, and when relevant, the magnitude of fractionations associated with other reaction and transfer pathways such as sulfur disproportionation (Jørgensen, 1977; Claypool et al., 1980; Garrels and Lerman, 1981; Berner, 1991; Strauss, 1993; Hurtgen et al., 2002, 2005; Canfield, 2004; Johnston et al., 2005a; Ono et al., 2006). Some of these studies have also suggested that non steady-state effects can introduce additional isotopic effects associated with material balance (Johnston et al., 2005a; Ono et al., 2006). In the first part of the following discussion we use steady-state sulfur cycle models to make inferences about the composition of seawater sulfate and sedimentary sulfide during IF deposition. Our models have a global component with a structure that is similar to that used in Johnston et al. (2005a) (Fig. 2a), but also includes local recycling of sulfur (Fig. 2b). In the second part of the discussion we make inferences about an expanded steady-state model (Fig. 2c) and a basic non steady-state system. Here, we draw on a combination of Rayleigh (e.g., Goldhaber and Kaplan, 1975) and mixing effects to gather information about the behavior of non steady-state systems.

4.1. Implications of the steady-state box model approach

The average composition of the source of sulfur for the oceanic sulfur cycle is thought to have an isotopic composition near, or slightly more enriched (<5‰ in $\delta^{34}S$) than that of CDT ($\delta^{33}S \approx 0$, $\delta^{34}S \approx 0$, and $\delta^{36}S \approx 0$) (Farquhar et al., 2002). When combined with constraints imposed by conservation of mass, the dominant fractionations in the surface sulfur cycle produce ^{34}S-depleted reservoirs of reduced sulfur (i.e. pyrite) and ^{34}S-enriched reservoirs of oxidized sulfur (i.e. sulfate). The observation that a majority of the sulfide data (35 of 38) from the successions examined here has positive delta values (are ^{34}S-enriched) indicates that the global sulfur sink (Fig. 2a) is not represented by this sample set. Observations of ^{34}S-enriched sulfide minerals have also been described in other Proterozoic shales (e.g., Walker and Bimblecombe, 1985; Hayes et al., 1992; Hayes, 1993; Shen et al., 2002, 2003; Canfield, 2004). Hayes et al. (1992) suggested that the lack of ^{34}S-depleted sulfides at this time reflects poor preservation of deep-water settings, where isotopic fractionation associated with sulfate reduction would have been large. Those authors suggest that lower rates of sulfate reduction in deep water settings would facilitate larger isotopic fractionations and the production of ^{34}S-depleted sulfide. These sulfides would likely be subducted and lost from the surface record (Canfield, 2004). Conversely, continental shelf and intracratonic basin settings, which represent much of the sampled record during these time intervals, and where organic carbon is readily available, are locations where sulfate reduction rates are assumed high and where near quantitative reduction of available sulfate is feasible. This would result in sedimentary sulfides with isotopic compositions near that of seawater sulfate, or in the case of the Proterozoic, between 0 and 20‰ in $\delta^{34}S$. We suggest that our data reflect the operation of a (basin-scale) sub-cycle similar to that presented in Fig. 2b. In this model, and consistent with the Hayes et al. (1992) model, the global cycle produces an oceanic sulfate reservoir with positive $\delta^{34}S$ (^{34}S-enriched)

Fig. 3. Triple isotope plots illustrating the steady-state sulfur cycle modeling solutions for the isotopic composition of sulfate and sulfide. Fractionation factors are derived from experiments with SRP conducted by Johnston et al. (2005b). The fields outlined in black represent a sulfur cycle with only SRP active, whereas fields outlined in gray have both SRP and SDP present. These models are extended versions of those presented in Johnston et al. (2005a), with 'SRP-SDP' predictions incorporating the re-oxidation of sulfide to sulfate (not shown in Fig. 2). The position along each respective curve represents the fraction of pyrite being buried (f_{py} in Johnston et al., 2005a). In the case of the sulfate curve, the intercept represents no pyrite burial with pyrite burial increasing to 100% as you move away from the origin to the right. Due to mass balance, the pyrite curve is demarcated in a similar manner with no pyrite burial at the left most point on the curve, and increasing towards 100% pyrite burial as you approach the origin. In all cases, sulfate and sulfide predictions evolve away from the origin since we assume a continental/riverine flux that is isotopically similar to bulk Earth ($\delta^{3i}S \sim 0‰$). All modeling represents steady-state box modeling of the global sulfur cycle (see Fig. 2). (a) The model structure presented in terms of $\Delta^{33}S$ versus $\delta^{34}S$, where lines extending towards positive $\delta^{34}S$ values represent predictions for seawater sulfate and lines extending towards negative $\delta^{34}S$ represent sulfide predictions. (b) Similar to the model fields presented in 3A, but with $\Delta^{36}S$ and $\delta^{34}S$, all else remains unchanged. (c) A triple isotope plot of $\Delta^{33}S$ and $\Delta^{36}S$. The fields extending into the second quadrant are sulfate predictions, whereas fields in quadrant four represent sulfide predictions. Also included is a model prediction (line slope −6.85) from Ono et al. (2006) for mass-dependent systems and a semi-quantitative ellipse that simplifies the graphical prediction of all the models. All other models parameters are the same as those discussed above.

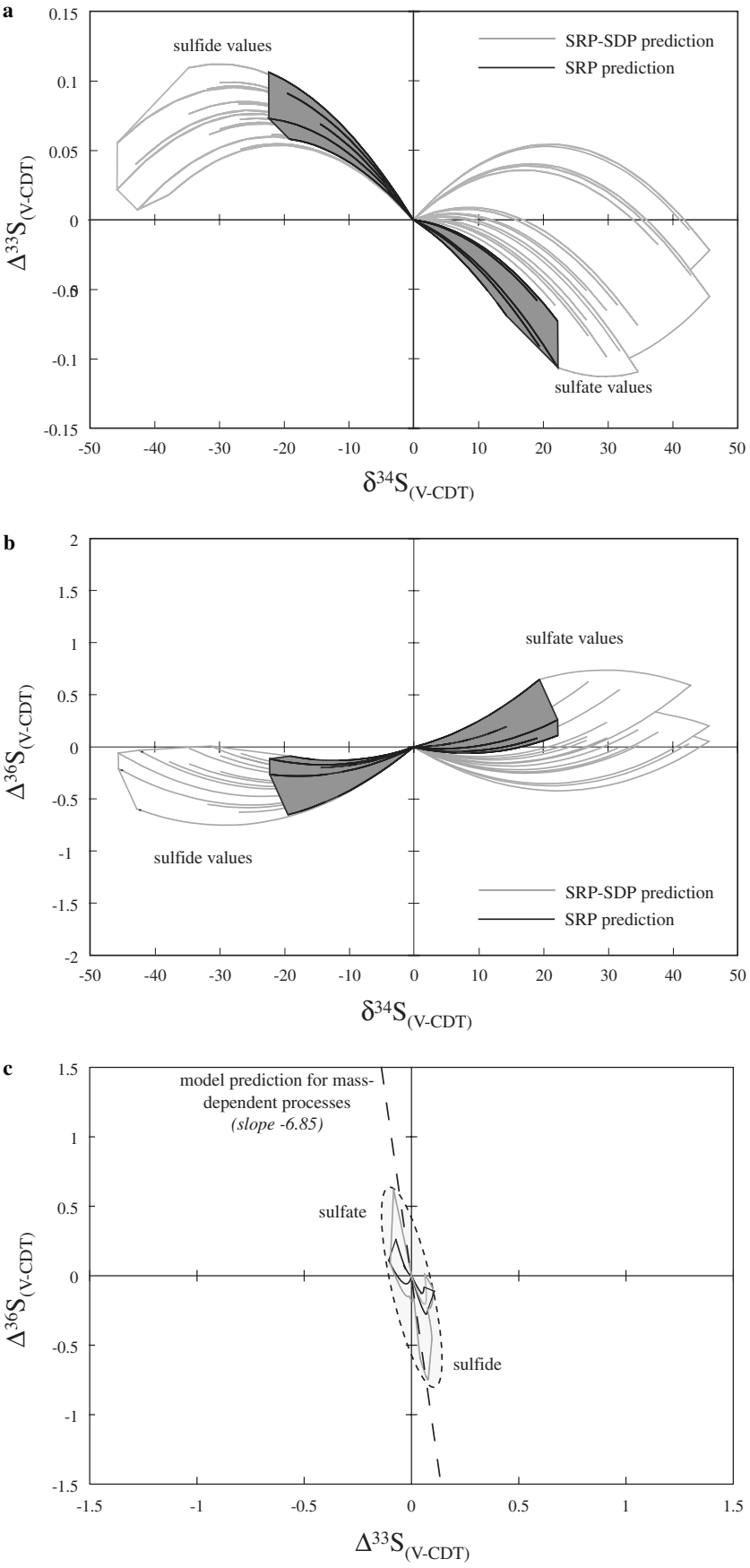
a
sulfide values
SRP-SDP prediction
SRP prediction
sulfate values
$\Delta^{33}S_{(V\text{-}CDT)}$
$\delta^{34}S_{(V\text{-}CDT)}$
b
sulfate values
sulfide values
SRP-SDP prediction
SRP prediction
$\Delta^{36}S_{(V\text{-}CDT)}$
$\delta^{34}S_{(V\text{-}CDT)}$
c
model prediction for mass-dependent processes
(slope -6.85)
sulfate
sulfide
$\Delta^{36}S_{(V\text{-}CDT)}$
$\Delta^{33}S_{(V\text{-}CDT)}$

that serves as the source pool for the basin-scale sub-cycle, thus allowing for the production of positive $\delta^{34}S$ sulfides on the shelves or shallower water settings.

4.2. The oceanic sulfate reservoir

The isotopic composition of the global oceanic sulfate reservoir during the late Paleoproterozoic remains poorly constrained. Traditional approaches to assess the isotopic composition of the past oceanic sulfate reservoir have been through direct analyses of proxies for oceanic sulfate (e.g., evaporite sulfate, carbonate associated sulfate, marine barite; Holser et al., 1979; Claypool et al., 1980; Burdett et al., 1989; Southwick and Morey, 1991, 1993; Paytan et al., 1998, 2004; Lyons et al., 2004; Turchyn and Schrag, 2004) and models of the sulfur cycle, which often rely on sulfide data (Canfield and Teske, 1996; Canfield, 2001). In recent studies by Johnston et al. (2005a) and Ono et al. (2006), the composition of the oceanic sulfate reservoir has also been evaluated using oceanic box models. These authors argue that the composition of oceanic sulfate will occupy an isotopic field that extends from the composition of the sulfate source to the oceans (roughly zero) to more positive $\delta^{34}S$ and variable but small positive and negative $\Delta^{33}S$ and $\Delta^{36}S$ values due to the continued removal of isotopically fractionated sulfide.

An expanded version of model predictions from Johnston et al. (2005a) is presented in Fig. 3(a–c). Whereas our earlier treatment focused on predicting the isotopic composition of seawater sulfate, the current treatment has been expanded to include predictions for the isotopic composition of sulfides. An assumption built into our model results is that the isotopic composition of the sulfur entering the system is roughly zero, and use microbial fractionation factors from Johnston et al. (2005b). Model interpretations do not change with small variations (up to ~5‰ in $\delta^{34}S$) in the composition of the sulfur source to the oceans. The model results define an "SRP field" (sulfate reducing prokaryote) representing a sulfur cycle with only active sulfate reduction and a "SRP-SDP field" (sulfur disproportionating prokaryote) representing the predictions for a sulfur cycle with contributions from both sulfate reducers and sulfur disproportionators. The isotopic field defined by a sulfur cycle with only sulfate-reducing microorganisms occupies a smaller region of predicted isotopic compositions than if other microbial processes, such as sulfur disproportionation, are active as well (see Johnston et al., 2005a). Previous studies suggest that only sulfate reducers operated within the sulfur cycle during the late Paleoproterozoic (Canfield and Teske, 1996; Canfield, 1998; Johnston et al., 2005a), suggesting that the smaller SRP field defines the range of compositions for oceanic sulfate at that time.

We use this model to provide a context for interpreting isotopic data for sulfides from the Gunflint, Biwabik, Trommald, and Mahnomen Formations. The steady-state box model would reproduce our IF sulfide data using fractionations associated with only sulfate reducing microorganisms and a fitted composition for oceanic sulfate of $\delta^{34}S \sim 17‰$, $\Delta^{33}S \sim -0.085‰$, and $\Delta^{36}S \sim 0.60‰$ (Fig. 4), which is the minimum estimate (in $\delta^{34}S$ and $\Delta^{36}S$, maximum in $\Delta^{33}S$) to satisfy the data. This prediction also supports the lack of a prominent isotopic contribution from SDP at this time. The validity of our estimate for the isotopic composition of the seawater sulfate reservoir hinges on the appropriateness of the model approach, but it also illustrates a new type of constraint for seawater sulfate compositions. This treatment provides a seawater sulfate composition that is not only consistent with earlier predictions of the $\delta^{34}S$ of Paleoproterozoic seawater sulfate (Strauss, 2004; Gellatly and Lyons, 2005), but consistent in ^{33}S and ^{36}S with our predictions from steady-state global box models (see position of sulfate field Fig. 3a versus the composition suggested for the period of BIF deposition: Fig. 4). Similar steady-state modeling cannot explain the significant scatter of the Rove Fm. sulfide data, thus a prediction of the associated seawater sulfate composition is not appropriate.

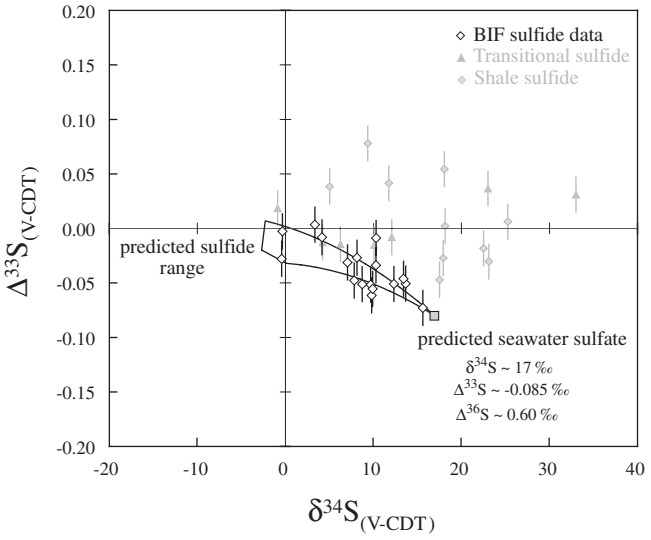

Fig. 4. Steady-state modeling results for a sulfur cycle with only active sulfate reducers. The models and data are represented on a $\Delta^{33}S$ and $\delta^{34}S$ plots (in ‰), however the same treatment can be performed using axes seen in (Fig. 3 b and c) with the conclusions remaining unchanged. The inclusion of a sub-cycle can shift the isotopic predictions, such that the sulfide and sulfate fields would not evolve away from a continental composition (original source pool; seen in Fig. 3), but would be rooted from a composition within the original seawater sulfate field (new source pool). In this case, global processes would be controlling the isotopic composition of the overlying seawater, but local effects are controlling the isotopic composition of the sedimentary sulfides in the sediment column. White diamonds represent IF sulfide data (with 2σ errors), while all other data is in light gray. The black lines represent the global predictions for a sulfur cycle with only SRP active and are rooted at the predicted seawater sulfate composition (gray square). This seawater sulfate prediction is non-unique and falls within the range predicted by Fig. 3a (an experimentally constrained field), and the theoretical predictions of Farquhar et al. (2003). Since the model adequately encompasses the data, we suggest that these sulfides are derived from the microbially (SRP) reduction of porewater sulfate within a sediment column under steady state conditions.

4.3. Iron formation environments

We interpret our IF data to reflect operation of a localized sulfur sub-cycle linked to the IF depositional environment (i.e. pore-water sulfate and local sedimentary sulfide) (Fig. 5). We envision the overlying seawater sulfate infiltrating the sediment column where microbial reduction of pore-water sulfate would generate sulfide that was captured as pyrite. In this environment, the small (~10‰) $\delta^{34}S$ fractionations between our model prediction for seawater sulfate and the measured sedimentary sulfide indicate either a high fraction of pore-water sulfate sulfur was reduced and captured as pyrite (local $f_{py} \rightarrow 1$, where local f_{py} is the ratio of pyrite sulfur to sulfur infiltrating as pore-water sulfate), or low pore-water sulfate concentrations. The high Fe-content of the sediments, coupled with low organic matter contents, suggest that lowered pore-water sulfate concentrations was most likely the limiting constituent in this environment (Habicht et al., 2002). The requisite source of Fe for pyrite formation is taken to be similar to other Superior-type IFs, which are thought to sample water derived from a deep ferruginous ocean, and where a majority of the ferrous iron would be chemically or microbially oxidized on the shelf (e.g. Derry et al., 1992).

4.4. Transitional environments

The suite of samples that lie between the underlying IF and the overlying euxinic shales of the upper Rove Formation were grouped by Poulton et al. (2004) on the basis of evidence from Fe-speciation work and designated as "transitional." The transitional nature of the depositional environment from which these samples were derived is further supported by the sulfur isotope data for this horizon, which straddles both the field defined by the Gunflint IF and the field defined by the overlying euxinic Rove Formation shale. The two lowermost samples in the transitional Rove Formation shales fall within the steady-state IF field, suggesting an initial consistency with the underlying IF data (i.e. deposition under ferruginous water column conditions). Data for immediately overlying samples diverge from the IF field and fall within the field for the euxinic Rove Formation shales. Further up-column, there is a brief return to coincidence with the IF field before the data terminally diverge to occupy the euxinic shale field. Noteworthy is that the 'transitional' samples overly the Gunflint/Rove disconformity, suggesting that the change in ocean chemistry or the establishment of a different basin scale sulfur cycle (discussed below) captured by these samples, post-dated the refilling of the Animike Basin, roughly 40 Ma after the deposition of the underlying iron formations.

4.5. Euxinic shale environment

The large amount of isotopic variability for the euxinic Rove Formation sulfides appears to be independent of stratigraphic position, cannot be explained by the inclusion of active SDP, and is inconsistent with the box model approach described in Fig. 2b. Similarly, the isotopic data for euxinic Rove sulfide occupy an area to the right of the sulfide field presented in Fig. 4. This observation leads us to consider the possible role of other effects within the euxinic Rove Fm. sulfur cycle. Two recent studies have described how removal of sulfide by Rayleigh fractionation processes can produce sulfur isotope compositions for

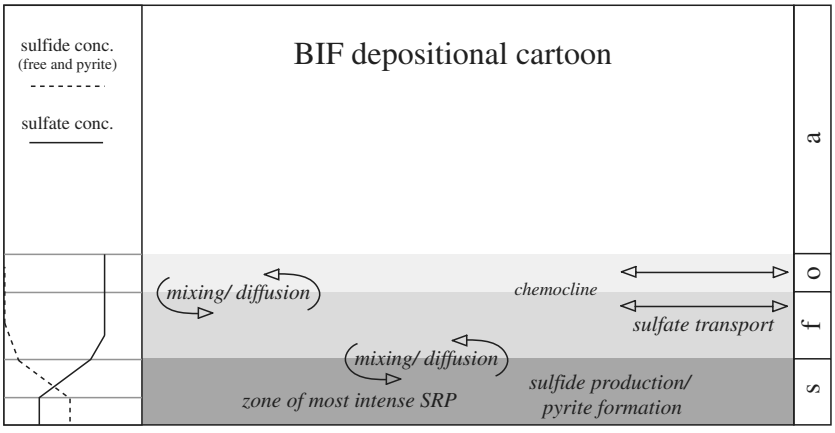

Fig. 5. A cartoon representing the envisioned IF depositional environment. The focus of this graphic is to constrain the cycling of sulfur through the system, and in doing so, other important elements and cycles may be underappreciated. In the right-most column, a, atmosphere; o, oxic ocean; f, ferruginous ocean; and s, sediments. This environment is interpreted to have a shallow, stratified water column with a component of horizontal (possibly wind/upwelling driven) transport. There would likely be significant oxic/anoxic interaction at the chemocline, with the zone of most intense SRP activity and pyrite production in the upper portions of the sediments, where organic material would most readily accumulate. The lifetime of sulfide in this system would be very short, as the available iron would quickly scavenge the free sulfide for Fe–S formation (and later pyrite). The profiles at left represent speculative ion profiles for two different sulfur species (sulfate and sulfide). The sulfate concentration would remain relatively constant until entering the lower portion of the water column, where the compositional gradients extending from the sediment system could draw down sulfate. This is a function of the most prominent sulfate sink being in the sediments. In the sediments, sulfate would be expected to decrease through the zone of active sulfate reduction and level off as methanogensis begins to dominate. The sulfide profile is a reflection of the sulfate prediction.

sulfate and sulfide that migrate to positive $\delta^{34}S$ with only small changes of $\Delta^{33}S$ (Johnston et al., 2005a; Ono et al., 2006). Similar effects may be produced in systems at steady-state with continuous sulfide loss, or in systems where changes in the source or sink terms have resulted in a non steady-state condition. We will discuss both the possibility for a non steady-state explanation for the euxinic Rove Fm. data, as well as the possibility that the data may be explained by a steady-state sulfur cycle with continuous loss of sulfide.

4.5.1. Possibility of a non steady-state sulfur cycle

Non steady-state conditions, of which Rayleigh effects are a limit, arise when variability in either the source or the sink reactions leads to a significant fluctuation in the size of one or more of the sulfur pools. We consider the temporal variability in seawater sulfate concentration as a function of the sum of fluxes in and fluxes out. The isotopic ratio of these fluxes results in the definition of a fractionation factor for the process. Thus, the isotopic consequence of a non steady-state depends on the fractionation between reservoirs and the magnitude of the change in reservoir size. These can be described by a combination of Rayleigh effects and mixing. In Fig. 6 we illustrate the way that a one-box system responds when the source flux decreases relative to the sink flux. In this system, the initial isotopic evolution follows a trajectory defined by conventional Rayleigh fractionation ($R_f = R_0 f^{(\alpha-1)}$, where f is the fraction of Rayleigh distillation, and R_f and R_0 are the isotopic ratios for the instantaneous composition at fraction f and for $f = 0$) (Fig. 6). As the size of the pool continues to change, the predicted isotopic evolution begins to loop back around towards the starting composition as a function of mass balance (noted as 'mixing (recovery) loops'). This treatment predicts a drastic initial isotopic evolution as a response to non steady-state conditions, but a slow and less isotopically drastic response as the system reaches a new steady state.

In order for a non steady-state interpretation of the euxinic Rove Fm. sulfide data to be valid, it must explain the general geological and geochemical features of the euxinic Rove shale. Those features include the interpretation that deposition occurred in a marine setting, and that large (tens of ‰) ^{34}S enrichments occur throughout about ~40 m of stratigraphic section. Given the measured fractionations (>20‰ in $\delta^{34}S$ and highly variable $\Delta^{33}S$ and $\Delta^{36}S$), the magnitude of the non-steady state effects for the Rove Fm. would require a process capable of generating significant changes in the size of the sulfate pool. This is because in order for a Rayleigh-like process to produce the observed effects, a significant fraction of the local sulfate reservoir (either bottom water sulfate or pore-water sulfate) must have been removed. This estimate may represent a lower limit, since this isotopic variation is captured in the sulfide, rather than sulfate, pool. A standing pool of sulfide in a sulfidic water column has the potential to damp the magnitude of isotopic signals that are transferred to it from the sulfate pool. For example, if 10's of μM sulfide are produced and assimilated into a standing sulfide pool of 100's of μM sulfide, the isotopic contribution of that most recent addition will not be fully expressed, whereas if there was no standing sulfide reservoir, the composition of the recently produced sulfide would be representative of the standing pool and could then be captured as pyrite.

Prior studies have suggested that some non steady-state effects may accompany the geographic restriction of

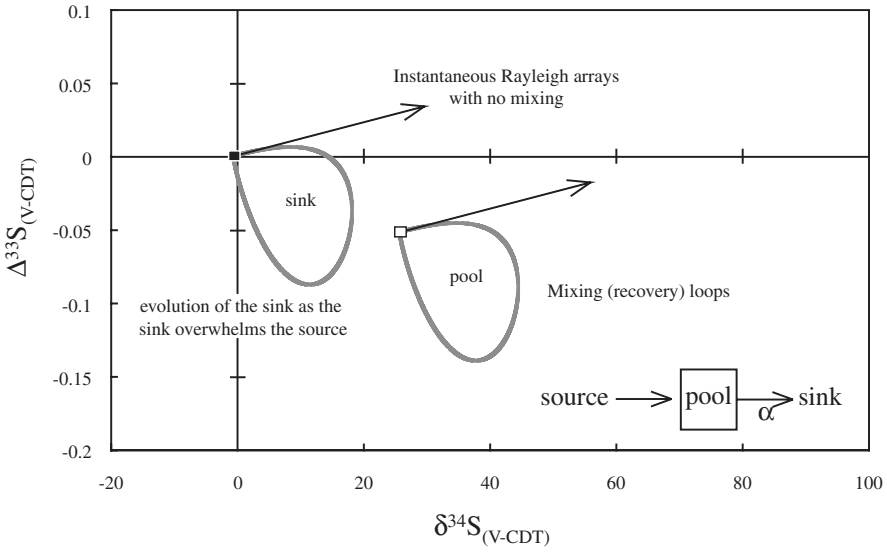

Fig. 6. A triple isotope plot describing the consequences of Rayleigh fractionation and mixing for the simple one box model presented in the lower corner of the figure. The black and white boxes are the steady state predictions for the compositions of the sink and pool respectively. The Rayleigh fractionation trajectories (straight arrows) constrain the initial direction that the loops (which include mass balance considerations) proceed in. The right most loop represents the evolving composition of the "pool," whereas the left most loop represents the evolving composition of the "sink", and is offset by a fractionation factor (α). Plotted is the scenario where the sink overwhelms the source.

a basin, with episodic re-supply from a sulfate source (e.g., Johnston et al., 2005a). We do not favor this for the Rove Formation because it has been interpreted to have been deposited in a marine environment, and thus communicating with the open ocean. As an alternative, we explore the possibility that the euxinic Rove Formation data reflect the normal operation of a low sulfate marine environment. We focus on two parts of this system, (1) the water column and (2) the underlying sediments.

High rates of sulfate reduction are common for organic rich sedimentary environments. Thus, it may be possible, given increased organic material, for euxinic water column sulfate reduction rates to consume a significant proportion of water column sulfate and induce a non steady-state behavior within the system. This type of situation can be described using a simple expression and observed rates for modern water column processes. We calculate steady-state, 1D penetration depths to gain an 'order of magnitude' estimate of how sulfate concentrations might vary as a function of overlying water column depths. We begin with a simple diffusion length-scale expression, where $L \sim \sqrt{Dt}$ (or length is related to the square root of diffusion multiplied by time). However, if we make the assumption that the characteristic timescales of the system are set by sulfate reduction rates (SRR), which is reasonable, we can substitute time (t) with the expression: [boundary concentration/sulfate reduction rate]. This is easier to understand when considering units, where boundary concentrations are reported in moles per liter (M), and sulfate reduction rates are reported in moles per liter per unit time (time = M/[M/time]). We run this calculation using low sulfate concentrations (1–4 mM), Black Sea water column mixing rates from Neretin et al. (2001) (0.5–3 cm^2/s) as a proxy for effective diffusivity, and for sulfate reduction rates of 1 μM/day which are at the high end of those reported for euxinic water columns (e.g., 0.0035–1.569 μM/day; Il'chencko and Sorokin, 1991; Jørgensen et al., 1991; Albert et al., 1995; Neretin et al., 2001; Sørensen and Canfield, 2004). Our results indicate that sulfate concentrations will approach zero at depths between ~50 and 350 m below the chemocline, which spans the inferred water column depths overlying the Rove Fm. As sulfate reduction rates increase, the water column depth required to remove significant amounts of sulfate decreases. Sørensen and Canfield (2004) observed a rate enhancement when water column samples were augmented with acetate and lactate. It has also been argued (Logan et al., 1995) that concentrations of suspended organic carbon (dissolved and particulate) were higher in the Proterozoic, which they argue would have fostered increased rates of water column sulfate reduction during that period. Both suggestions indicate that significant water column sulfate removal is likely under supposed Proterozoic shelf conditions (euxinic with high organic carbon). These predictions assume that there is not significant lateral transport of sulfate-rich water onto the shelf, but acknowledging that lateral homogeneity is more likely in closed basins or where continental shelves are extensive.

The development of a sulfate-limited system, which is modeled as a non steady-state response in the euxinic Rove Formation sulfur cycle, may also have been initiated as a result of changes in the rates of sulfate uptake by sediments. Considerations of the contribution of active sulfate reduction in the underlying sediments, and the role that this sulfate sink can play in water column chemistry, must also be considered. In low sulfate concentration water column-sediment systems, variations in sulfate reduction may influence the size of the water column sulfate pool. The depths inferred for the Rove Formation depositional environments (~100 to 200 m) are on the same order as the characteristic diffusion length-scales described using the same equation described above ($\sqrt{Dt}$) and using the above listed mixing rates. Given typical rates for uptake of sulfate measured in modern sedimentary systems (~0.2 to 50 mol/m^2yr) (e.g., Jørgensen, 1977), it is predicted that there will be a significant extension of the sedimentary/water column boundary layer that would result in sulfate draw down in the water column. For example, a 100 m by 1 m^2 water column with 1 mM of sulfate contains only 100 mol of total sulfate, and variability within the range of observed rates of sedimentary sulfate uptake will have a significant impact on the size (2–50% change) and isotopic composition of the sulfate pool in this system. This interpretation assumes lateral homogeneity aided by bottom water currents, and the presence of rip-up interclasts suggests that bottom water currents were, at the very least, sporadic. However, this also depends on the lateral extent (scale) of the system and whether these water currents introduced sulfate-rich water from other deep-water sources. Since active communities of sedimentary sulfate reducers (or the physical process producing water column drawdown of sulfate concentrations) are largely independent of small variances in bottom water currents, the general treatment presented above should apply. In essence, a low sulfate water column can easily become sulfate limited when sedimentary SRP communities are present, and especially where the water column is shallower and organic inputs high, such as in the Rove Fm.

For variations in the intensity of water column sulfate reduction rates, or variations in the intensity of the sedimentary sulfate drawdown mechanism to be feasible explanations, these rates must vary on timescales that are comparable to the response time of the Rove Formation sulfur cycle. This will depend, in part, on water column mixing rates, but will also be influenced by changes in controls on sulfate reduction rates, such as ambient water temperatures and nutrient availability. We infer that the Rove Formation water column had a short response time (seasonal to yearly), which we estimated using the length-scale expression presented above. Another issue that must be considered in evaluating the plausibility of a sulfate-limited explanation for the Rove Formation data is related to the size of the standing pool of water column sulfide. A large

standing sulfide pool would have the potential to damp the isotopic signal of the sulfide reservoir. This leads us to suggest that although these scenarios have the potential to produce variations in the water column sulfate concentration profiles, they would not be sufficient to produce the sustained and significant Rayleigh isotopic signal observed for the sulfides. For these reasons, we do not favor this interpretation.

4.5.2. Possibility of a sulfur cycle with continuous sulfide loss

An alternative model we propose for the euxinic Rove Formation sulfide data is a steady-state sulfur cycle that includes a significant and continuous loss of sulfide. A box model with this structure is presented in Fig. 2c. The field of sulfide compositions that can be produced by this box model using experimentally-determined sulfur isotope fractionations (e.g., Farquhar et al., 2003; Johnston et al., 2005b) is plotted in Fig. 7. In general, as more sulfate and sulfide boxes are added to the model, mass-balance requires that the composition of sulfate moves to the lower right of Fig. 7, due to the removal of isotopically depleted sulfides. Sulfide removal can occur through a number of processes, such as oxidation, burial, and various transports pathways out of the system. Fig. 7a presents all the data with the steady-state predictions for the isotopic composition of seawater sulfate (right field) and global sedimentary sulfide, assuming only one sulfide sink (left field). Fig. 7b show the evolution of predicted sulfide compositions as additional sulfide sinks are added, with Fig. 7b representing a scenario with four sulfide sinks (global pyrite plus all sulfide sinks presented in Fig. 2c). Strictly speaking, the model is an incremental batch loss process rather than a Rayleigh process, but the expansion of the sulfide field reflects the loss of ^{32}S-enriched sulfur from the system, as it does in Rayleigh systems. More complex models such as those with additional steps for sulfide loss (Fig. 7b) are capable of producing an even larger field for sulfide isotopic compositions and predict isotopic compositions that more closely match that of the Rove Fm. data. This style of explanation would not require the extreme situation required for Rayleigh effects, but only multiple sulfide sinks for the system. This explanation becomes even more achievable (i.e. less sinks required) if the fractionation associated with SRP increases (due to limited experimental data, the upper fractionation used in the modeling is ~27‰ in δ^{34}S). For the model represented in Fig. 7 to work, it must allow a significant loss of sulfide from the system (>50%), a fraction that is significantly higher than the fraction of sulfide lost to pyrite formation in the Black Sea (e.g., Neretin et al., 2001). Recently, Kump et al. (2005) suggested that upward excursions of the chemocline in the Proterozoic oceans may have ventilated sulfidic waters in upwelling zones, releasing hydrogen sulfide into the atmosphere. Evidence for a shallow chemocline in some Paleoproterozoic environments is given by recent biomarker evidence that placed the sulfidic/oxic chemocline within the photic zone of the McArthur basin (Brocks et al., 2005). Such a loss process may apply to the Rove Formation sulfur cycle, but would further require that sulfide delivered to the atmosphere be laterally transported away from the basin before returning to the oceanic sulfur cycle (as either sulfide, or more likely as sulfate). Transport implied by the Kump et al. (2005) model provides a way to remove this sulfur from the Rove Formation sulfur cycle; however the possibility also exists that the loss may be associated with lateral heterogeneity, where a gradual isotopic enrichment of seawater sulfate (due to the progressive removal of isotopically depleted sulfide) accompanies the transport of sulfate through the system. Further, reports of sulfide samples with strongly positive δ^{34}S from other middle Proterozoic sequences such as the Reward Formation, Wollogorang Formation, and Roper Group (e.g.,

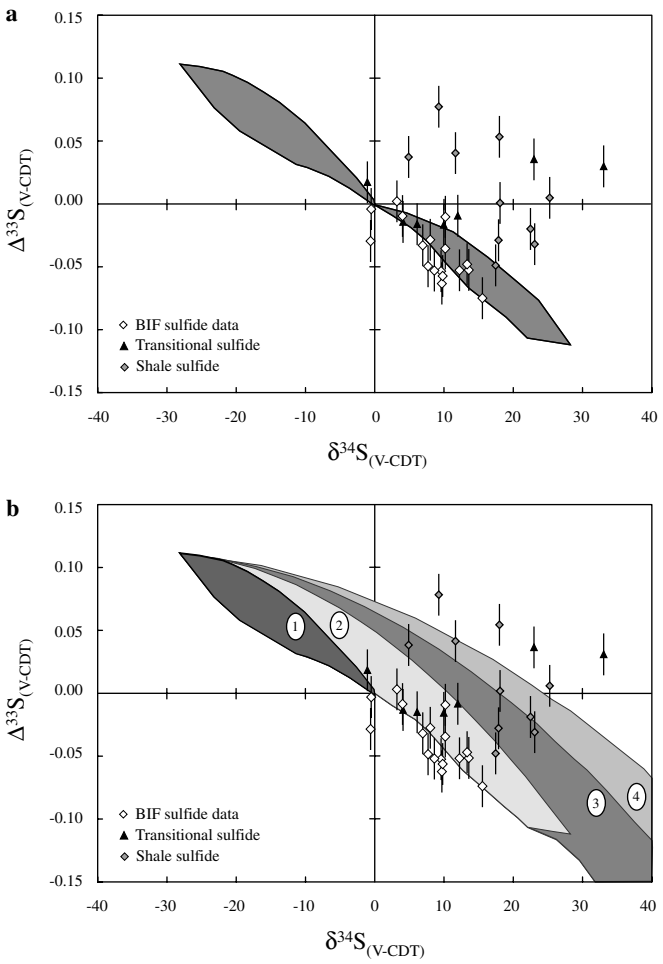

Fig. 7. A triple isotope plot of the sulfide data for the period of shale deposition. Iron formation data are represented by white diamonds, the transitional shale with black triangles and the euxinic shale with gray diamonds. All errors are 2σ. (a) A steady-state system with only one sulfide sink (global pyrite; labeled as 1), similar to that seen in Fig. 3a and with additional fractionation factors from Farquhar et al. (2003). The field extending towards the left represents sulfides whereas the field extending towards the right represents the sulfates in the system. (b) A scenario with four sulfide sinks, labeled 1–4 (the global sulfide, with all three additional sulfide sinks in Fig. 2c). It can be seen from the figure that as the number of sulfide sinks increases, steady state models can produce more enriched sulfide compositions.

Hayes et al., 1992; Hayes, 1993; Shen et al., 2002, 2003), may provide a link between our data and global mid-Proterozoic sulfur cycle that had a component of continuous sulfide loss. Tests for this hypothesis would include studies that include $\delta^{33}S$ and $\delta^{36}S$ in addition to $\delta^{34}S$ for these and other localities, where we would predict isotopic compositions similar to those seen in the Rove Formation.

A cartoon describing our interpretation of the Rove Fm sub-cycle is presented in Fig. 8. We suggest that the local sulfate reservoir is a combination of euxinic water column sulfate and pore-water sulfate. We envision the sulfate source to this system as the overlying oxic surface ocean seawater sulfate pool and sulfate from this overlying reservoir would vertically mix into the sulfidic portions of the water column and diffuse into underlying sediments. Sulfate reducing prokaryotes populating both the euxinic portions of the water column and the underlying sediments would contribute to the variability observed in the Rove, where fluctuations in the biological controls (temperature, nutrient fluxes and organic rain from surface environments) and sulfate delivery to the sulfidic parts of the sulfur cycle would have lead to development of non steady-state concentration effects, but only minor isotopic variations if the standing pool of water column sulfide was significant. Transport of sulfide out of the system, either as a result of horizontal transfer within the ocean, or as a result of ocean–atmosphere transfer of hydrogen sulfide, would leave the residual reservoir ^{34}S enriched and contribute to the positive $\delta^{34}S$ observed in the shale sulfide reservoir. As suggested above, the Rove Formation may not be unique, as similar processes may have operated in other middle Proterozoic settings.

4.6. Dispelling non mass-dependent contributions and calibrating a new relationship

The question of whether a sulfur isotopic composition is entirely the result of mass-dependent processes, or also possesses a component attributable to non mass-dependent chemistry, is not a trivial one when interpreting the Precambrian geologic record. Large (‰ scale) non mass-dependent isotopic signals have been observed in sulfur samples older than 2.45 billion years old. These observed effects have thus far been attributed to gas-phase photochemical reactions in a low O_2 atmosphere (e.g., Farquhar et al., 2000, 2001; Pavlov and Kasting, 2002; Farquhar and Wing, 2003, 2005; Mojzsis et al., 2003; Hu et al., 2003; Ono et al., 2003; Bekker et al., 2004; Papineau et al., 2005). Some workers have further argued for the persistence of small non mass-dependent signals into the Paleoproterozoic, where a resolvable, but much smaller signature remains (for samples with ages between 2.4 and 2.0 billion years old; Stage II of Farquhar et al., 2000; Farquhar and Wing, 2003, 2005). The samples studied here are slightly younger

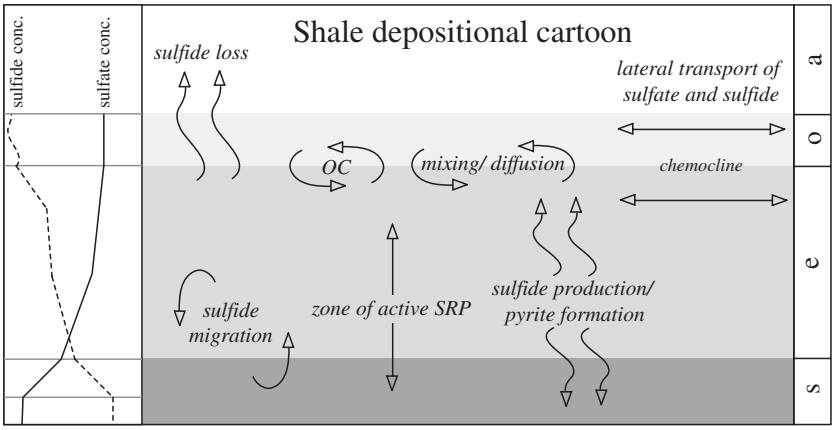

Fig. 8. A cartoon representing the envisioned shale depositional environment. The focus of this graphic is to constrain the cycling of sulfur through the system, and in doing so, other important elements and cycles may be underappreciated. In the right-most column, a, atmosphere, o, oxic ocean, e, sulfidic (or euxinic) ocean, and s, sediments. This environment is interpreted to have been deeper water than the IF environment, with a larger anoxic portion of the overall water column. In this scenario, lateral transport could move both sulfate and sulfide (sulfide in sulfidic waters). Sulfate reduction would be active in the water column of this environment, which makes this system inherently more dynamic (a sulfur sink in the water column with the capability of migrating). With this in mind, the recycling of organic carbon (OC) and the mixing/diffusion across the oxic/anoxic interface are of vital importance. Recent propositions even suggest that the chemocline could reach the surface of the ocean, venting sulfide directly to the atmosphere (Kump et al., 2005). The outgassing mechanism is a viable solution for satisfying our sulfide data (see text for more detail). The zone of most intense SRP activity and pyrite production would still remain in the upper portions of the sediments, but sulfate reduction would inhabit the water column. The lifetime of sulfide in this system would be much longer than in the IF setting, as the available sulfide would overwhelm the available iron. The profiles at left represent speculative ion profiles for two different sulfur species (sulfate and sulfide). The sulfate concentration would begin to decrease in the euxinic portion of the water column as a function of low, but present rates of microbial sulfate reduction. A similar extension of the compositional gradient would draw down sulfate more quickly as the sediment/water interface is approached. In the sediments, sulfate would be expected to decrease through the zone of active sulfate reduction and level off as methanogensis begins to dominate. The sulfide profile is similar, but not a direct reflection. Potential outgassing to the atmosphere requires a variable amount of sulfide in the surface ocean, which is represented by the wavy line atop the sulfide concentration profile. Sulfide would increase quickly below the chemocline as a function of the diffusive boundary layer with the overlying oxic waters, and due to more labile organics near the surface, followed by slow accumulation through mid-depths. The compositional gradient produced in the sediment system would still intrude into the water column, causing an increase in sulfide near this interface. Below this, sulfide concentrations stabilize and are largely represented by pyrite.

than those defining Stage II, but can serve to test the proposed lack of non mass-dependent signatures and presence of a mass-dependent surface sulfur cycle at the time of deposition.

Previous research has suggested that the relationships between $\delta^{33}S$ and $\delta^{34}S$ ($\delta^{33}S/\delta^{34}S$) and $\Delta^{36}S$ and $\Delta^{33}S$ ($\Delta^{36}S/\Delta^{33}S$) can be used to distinguish between fractionations produced by mass-dependent and non mass-dependent processes (Farquhar and Wing, 2003, 2005; Wing et al., 2004; Ono et al., 2006). Ono et al. (2006) recently argued that isotope effects associated with mass-dependent (MD) geochemical systems would yield a $\delta^{33}S/\delta^{34}S \sim 0.512$–$0.515$ and a $\Delta^{36}S/\Delta^{33}S$ relationship that would converge on a value of ~ -7. Non mass-dependent evidence suggests a much more variable $\Delta^{36}S/\Delta^{33}S$ (ranging from $\Delta^{36}S/\Delta^{33}S$ of -10.36 [Zmolek et al., 1999] to 1.8 [Farquhar et al., 2001]), however observation of Archean samples suggests a terrestrial record of ~ -1. Our data are consistent with the mass-dependent criteria (e.g., Fig. 9), and suggest that non mass-dependent isotopic fractionation effects, and non mass-dependent detrital contributions, can be ruled out at the time that this succession was deposited. The consistent nonzero intercept for the $\Delta^{36}S/\Delta^{33}S$ of ~ 0.3 suggests a consistent sulfur source to the system with a composition different from our normalization V-CDT. We also provide a steady-state model prediction (Figs. 3c, Fig. 9) that demonstrates the consistency of the IF data with such predictions. While our observations are consistent with prevailing hypotheses about modest levels of oxygen in the early to middle Proterozoic, they provide a constraint on the extent of the hypothesized Stage II, which marks the transition period between the non mass-dependent world and one more like the modern. Important to understanding element cycles at this time is accepting the difference between what is implied by Stage II in the sulfur and iron isotope records (Farquhar et al., 2000; Rouxel et al., 2005), as the S-record is based on contributions from low O_2 settings and the associated processes whereas the Fe-record is based on oceanic redox conditions.

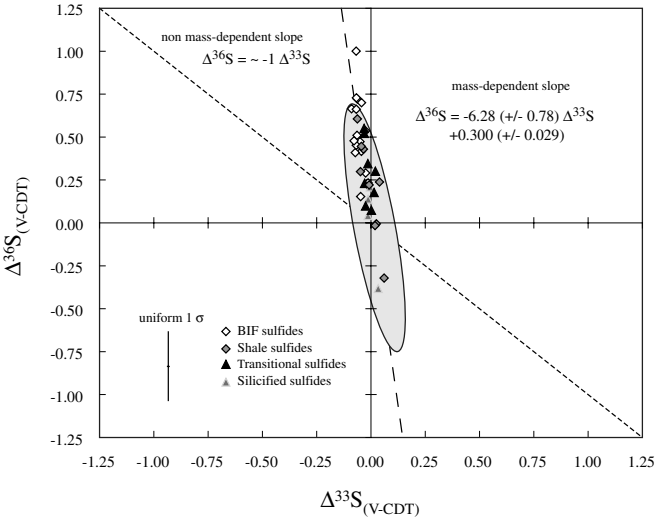

Fig. 9. The data plotted in terms of $\Delta^{36}S$ and $\Delta^{33}S$ plot (in ‰). Also included is the model ellipse from Fig. 3c (solid gray ellipse). In the figure, the BIF sulfides are represented by white diamonds, the shale sulfides are gray diamonds, the transitional sulfides are black triangles, and the silicified samples are light triangles. A representative error bar is reported in the bottom left. The short dashed line is an observational trend noted in Archean sediments (see text for details and citations) and plots with a slope of ~ -1. Also plotted is a regression through the data, which produces a trend of slope -6.28. The observed slope for our data is within 1σ of predictions from Ono et al. (2006), who predicted a slope of -6.85, and is satisfied when plotted with the steady-state modeling treatments (gray ellipse). The observed consistency between mass-dependent predictions and our data, reinforced by the gross deviation from the observed Archean line, suggests that these samples were produced by only mass-dependent fractionation processes. We postulate that the observed small-scale variations are the result of a slight decoupling of ^{33}S and ^{36}S fractionations related to both the geochemical redistribution of material (accounted for both in this treatment and in Ono et al., 2006) and a biologically produced effect (modeled here). The later will be addressed in a subsequent study.

5. Conclusions

We have argued that the transition from ferruginous to sulfidic ocean conditions circa 1840 My ago is coincident with significant changes in the sulfur cycle. Despite these changes, our data do not require a significant change in seawater sulfate concentration at this transition. Our data and models suggest that during the period of IF deposition, the sulfur cycle fell under local diagenetic control and that seawater and pore-water sulfate reached an isotopic steady-state. Isotopic variability within this setting is interpreted as the result of changes in local pyrite burial associated with fluctuations in iron inputs and sulfate reducer activity. These modeling treatments also provide a new means of estimating the isotopic composition of seawater sulfate. This estimate is also consistent with a lack of prominent isotopic contributions from SDP at this time. Our data suggest that low seawater sulfate concentrations, coupled with active microbial sulfate reduction and a euxinic water column, destabilized the sulfur cycle that dominated during IF deposition and ushered in a sulfur cycle during deposition of the Rove Formation that included loss of ^{34}S-depleted sulfide. The occurrence of positive $\delta^{34}S$ sulfides throughout the entire Rove Formation with $\Delta^{33}S$ that are consistent with a local loss process, and ^{34}S-enriched sulfides in other late Paleoproterozoic sequences leads to the suggestion the sustained loss process for ^{34}S-depleted sulfur was widespread. This may reflect outgassing of water column hydrogen sulfide to the atmosphere (Kump et al., 2005). Further studies of all four sulfur isotopes from other Proterozoic, sulfide-bearing sulfidic successions should provide a test for this hypothesis. Our data suggest that the oscillations between different modes of the sulfur cycle from the steady-state regime associated with the Gunflint Formation, Biwibik Formation, Trommald Formation, and Mahnomen Formation, to the continuous loss regime associated with the Rove Formation was not immediate

and that at least one reversal preceded the permanent establishment of sulfidic conditions. We recognize that the connections between biology, ocean mixing, ocean-atmosphere exchange, and basin-scale cycling of sulfur during the Proterozoic remain to be better explored. However, the possibility of continuous loss of hydrogen sulfide to the atmosphere, coupled with the potential for a pervasive shallow chemocline, would have undoubtedly influenced myriad elemental cycles and hindered the advancement/evolution of life through this time.

Acknowledgments

We thank L. Kump, Y. Shen, J. Amend, and one anonymous reviewer for constructive and insightful comments. We acknowledge support from NSF (EAR 0348382), NASA (NAG512350), the NASA Astrobiology Institute (D.T.J., BAW, J.F.), NAI Research fellowship (D.T.J.), National Science and Engineering Research Council of Canada (P.W.F.), and Danish National Research Foundation (Danmark's Grundforskningsfond; SWP, D.E.C.) for support of this research.

Associate editor: Jan P. Amend

References

Addison, W.D., Brumpton, G.R., Vallini, D.A., McNaughton, N.J., Davis, D.W., Kissin, S.A., Fralick, P.W., Hammond, A.L., 2005. Discovery of distal ejecta from the 1850 Ma Sudbury impact event. *Geology* **33** (3), 193–196.

Albert, D.B., Taylor, C., Martens, C.S., 1995. Sulfate reduction rates and low molecular-weight fatty-acid concentrations in the water column and surficial sediments of the Black-Sea. *Deep-Sea Res. Part I Oceanogr. Res. Papers* **42** (7), 1239–1260.

Arnold, G.L., Anbar, A.D., Barling, J., Lyons, T.W., 2004. Molybdenum isotope evidence for widespread anoxia in mid-proterozoic oceans. *Science* **304** (5667), 87–90.

Bekker, A., Holland, H.D., Wang, P.L., Rumble, D., Stein, H.J., Hannah, J.L., Coetzee, L.L., Beukes, N.J., 2004. Dating the rise of atmospheric oxygen. *Nature* **427** (6970), 117–120.

Berner, R.A., 1991. A model for atmospheric CO_2 over phanerozoic time. *Am. J. Sci.* **291** (4), 339–376.

Brocks, J.J., Love, G.D., Summons, R.E., Knoll, A.H., Logan, G.A., Bowden, S.A., 2005. Biomarker evidence for green and purple sulphur bacteria in a stratified Palaeoproterozoic sea. *Nature* **437** (7060), 866–870.

Burdett, J.W., Arthur, M.A., Richardson, M., 1989. A Neogene seawater sulfur isotope age curve from Calcareous Pelagic microfossils. *Earth Planet. Sci. Lett.* **94** (3-4), 189–198.

Canfield, D.E., 1998. A new model for Proterozoic ocean chemistry. *Nature* **396** (6710), 450–453.

Canfield, D.E., 2001. Biogeochemistry of sulfur isotopes. In: Valley, J.W., Cole, D.R. (Eds.), *Stable Isotope Geochemistry: Reviews in Mineralogy and Geochemistry,* pp. 607–636.

Canfield, D.E., 2004. The evolution of the Earth surface sulfur reservoir. *Am. J. Sci.* **304** (10), 839–861.

Canfield, D.E., Raiswell, R., Westrich, JT., Reaves, C.M., Berner, R.A., 1986. The use of chromium reduction in the analysis of reduced inorganic sulfur in sediments and shales. *Chem. Geol.* **54**, 149–155.

Canfield, D.E., Teske, A., 1996. Late Proterozoic rise in atmospheric oxygen concentration inferred from phylogenetic and sulphur-isotope studies. *Nature* **382**, 127–132.

Claypool, G.E., Holser, W.T., Kaplan, I.R., Sakai, H., Zak, I., 1980. The age curves of sulfur and oxygen isotopes in marine sulfate and their mutual interpretation. *Chem. Geol.* **28** (3–4), 199–260.

Derry, L.A., Kaufman, A.J., Jacobsen, S.B., 1992. Sedimentary cycling and environmental-change in the late proterozoic—evidence from stable and radiogenic isotopes. *Geochim. Cosmochim. Acta* **56** (3), 1317–1329.

Ding, T., Valkiers, S., Kipphardt, H., De Bievre, P., Taylor, P.D.P., Gonfiantini, R., Krouse, R., 2001. Calibrated sulfur isotope abundance ratios of three IAEA sulfur isotope reference materials and V-CDT with a reassessment of the atomic weight of sulfur. *Geochim. Cosmochim. Acta* **65** (15), 2433–2437.

Farquhar, J., Bao, H., Thiemens, H.M., 2000. Atmospheric influence of earth's earliest sulfur cycle. *Science* **289**, 756–759.

Farquhar, J., Savarino, J., Airieau, S., Thiemens, M.H., 2001. Observation of wavelength-sensitive mass-independent sulfur isotope effects during SO_2 photolysis: implications for the early atmosphere. *J. Geophys. Res. Planet.* **106** (E12), 32829–32839.

Farquhar, J., Wing, B.A., McKeegan, K.D., Harris, J.W., Cartigny, P., Thiemens, M.H., 2002. Mass-independent sulfur of inclusions in diamond and sulfur recycling on early earth. *Science* **298** (5602), 2369–2372.

Farquhar, J., Wing, B.A., 2003. Multiple sulfur isotopes and the evolution of the atmosphere. *Earth Planet. Sci. Lett.* **213**, 1–13.

Farquhar, J., Wing, B.A., 2005. The terrestrial record of stable sulphur isotopes: a review of the implications for the evolution of Earth's sulphur cycle. In: *Mineral Deposits and Earth Evolution.* Geological Society, London, Special Publication, 167–177.

Farquhar, J., Johnston, D.T., Wing, B.A., Habicht, K.S., Canfield, D.E., Airieau, S., Thiemens, M.H., 2003. Multiple sulfur isotopic interpretations of biosynthetic pathways: Implications for biological signatures in the sulfur isotope record. *Geobiology* **1**, 27–42.

Fralick, P.W., 1988. Microbial bioherms, lower proterozoic gunflint formation, Thunder Bay, Ontario. In: Geldsetzer, H.H.J., James, N.P., Tebbut, G.E., Reefs (Eds.), Canada and Adjacent Areas. *Canadian Society of Petroleum Geologists Memoir* 13, pp. 24–29.

Fralick, P.W., Barrett, T.J., 1995. Depositional controls on iron formation associations in Canada. In: Plint, A.G. (Ed.), Sedimentary Facies Analysis, *International Association of Sedimentologists Special Publication* 22, pp. 137–156.

Fralick, P.W., Davis, D.W., Kissin, S.A., 2002. The age of the Gunflint Formation, Ontario, Canada: single zircon U–Pb age determinations from reworked volcanic ash. *Can. J. Earth Sci.* **39**, 1085–1091.

Fralick, P.W., Miall, A.D., 1989. Sedimentology of the lower Huronian supergroup (early proterozoic), Elliot Lake, Ontario, Canada. *Sediment. Geol.* **63**, 127–153.

Gao, X., Thiemens, M.H., 1993. Isotopic composition and concentration of sulfur in carbonaceous chondrites. *Geochim. Cosmochim. Acta* **57** (13), 3159–3169.

Garrels, R.M., Lerman, A., 1981. Phanerozoic cycles of sedimentary carbon and sulfur. *Proc. Natl. Acad. Sci. USA Phys. Sci.* **78** (8), 4652–4656.

Gellatly, A.M., Lyons, T.W., 2005. Trace sulfate in mid proterozoic carbonates and the sulfur isotope record biospheric evolution. *Geochim. Cosmochim. Acta* **69** (15), 3813–3829.

Goldhaber, M.B., Kaplan, I.R., 1975. Controls and consequences of sulfate reduction rates in recent marine sediments. *Soil Sci.* **119** (1), 42–55.

Habicht, K.S., Gade, M., Thamdrup, B., Berg, P., Canfield, D.E., 2002. Calibration of sulfate levels in the Archean ocean. *Science* **298** (5602), 2372–2374.

Hayes, J.M., Lambert, I.B., Strauss, H., 1992. The sulfur isotopic record. In: Schopf, J.W., Klein, C. (Eds.), *The Proterozoic Biosphere, a Multidisciplinary Study*, pp. 129–132.

Hayes, J.M., 1993. Factors controlling C-13 contents of sedimentary organic-compounds—principles and evidence. *Mar. Geol.* **113** (1-2), 111–125.

Heamen, L., Easton, R.M., Hart, T.R., MacDonald, C.A., Fralick, P.W., Hollings, P., 2005. Proterozoic history of the Lake Nipigon area, Ontario: constraints from U–Pb zircon and baddelyite dating. *Ontario Exploration and Geoscience Symposium*, Toronto, Ontario, 12–14.

Hemming, S.R., McLennan, S.M., Hanson, G.N., 1995. Geochemical and Nd/Pb isotopic evidence for the provenance of the Early Proterozoic Virginia Formation, Minnesota. Implications for tectonic setting of the Animikie Basin. *J. Geol.* **103**, 147–168.

Hoffman, P.F., 1987. Early Proterozoic foredeeps, foredeep magmatism and Superior-type iron-formations of the Canadian shield. In: Kroner, A. (Ed.), Proterozoic Lithospheric Evolution, American Geophysical Union Series, vol. 17, pp. 85–98.

Holser, W.T., Kaplan, I.R., Sakai, H., Zak, I., 1979. Isotope geochemistry of oxygen in the sedimetnary sulfate cycle. *Chem. Geol.* **25** (1–2), 1–17.

Hu, G.X., Rumble, D., Wang, P.L., 2003. An ultraviolet laser microprobe for the in situ analysis of multisulfur isotopes and its use in measuring Archean sulfur isotope mass-independent anomalies. *Geochim. Cosmochim. Acta* **67** (17), 3101–3118.

Hulston, J.R., Thode, H.G., 1965. Cosmic ray produced ^{36}S and ^{33}S in metallic phase of iron meteorites. *J. Geophys. Res.* **70**, 4435–4442.

Hurtgen, M.T., Arthur, M.A., Suits, N.S., Kaufman, A.J., 2002. The sulfur isotopic composition of Neoproterozoic seawater sulfate: implications for a snowball Earth? *Earth Planet. Sci. Lett.* **203**, 413–429.

Hurtgen, M.T., Arthur, M.A., Galverson, G.P., 2005. Neoproterozoic sulfur isotopes, the evolution of microbial sulfur species, and the burial efficiency of sulfide as sedimentary pyrite. *Geology* **33** (1), 41–44.

Il'chencko, S.V., Sorokin, Y.I., 1991. K otsenke intensivnosti obrazovaniya serovodoroda v Chernom more (To the estimate of hydrogen sulfide production in the Black Sea). In: Vinogradov, M.E. (Ed.), *The Black Sea Ecosystem Variability: Natural and Anthropogenic Factors*. Nauka, Moscow, 73–77 (in Russian).

Johnston, D.T., Wing, B.A., Farquhar, J., Kaufman, A.J., Strauss, H., Lyons, T.W., Kah, L.C., Canfield, D.E., 2005a. Active microbial sulfur disproportionation in the Mesoproterozoic. *Science* **310**, 1477–1479.

Johnston, D.T., Farquhar, J., Wing, B.A., Kaufman, A.J., Canfield, D.E., Habicht, K.S., 2005b. Multiple sulfur isotope fractionation in biological systems. *Am. J. Sci.* **305**, 645–660.

Jørgensen, B.B., 1977. Sulfur cycle of coastal marine sediments. *Limnol. Oceanogr.* **22** (5), 814–832.

Jørgensen, B.B., Fossing, H., Wirsen, C.O., Jannasch, H.W., 1991. Sulfide oxidation in the anoxic Black-Sea Chemocline. *Deep-Sea Res. A Oceanogr. Res. Papers* **38**, S1083–S1103.

Krogh,T.E., Davis, D.W., Corfu, F., 1984. Precise U–Pb zircon and baddeleyite ages for the Sudbury area. In: Pye, E.G. (Ed.), *The Geology and Ore Deposits of the Sudbury Structure*. Ontario Geological Survey Special Vol., 1, pp. 431–446.

Krouse, H.R., Coplen, T.B., 1997. Reporting of relative sulfur isotope-ratio data (technical report). *Pure Appl. Chem.* **69** (2), 293–295.

Kump, L.R., Pavlov, A., Arthur, M.A., 2005. Massive release of hydrogen sulfide to the surface ocean and atmosphere during intervals of oceanic anoxia. *Geology* **33** (5), 397–400.

Logan, G.A., Hayes, J.M., Hieshima, G.B., Summons, R.E., 1995. Terminal proterozoic reorganization of biogeochemical cycles. *Nature* **376** (6535), 53–56.

Lucente, M.E., Morey, G.B., 1983. *Stratigraphy and sedimentology of the lower Proterozoic Verginia Formation*, Northern Minnesota. Minnesota Geological Survey Report of Investigations 28, p. 28.

Lyons, T.W., Walter, L.M., Gellatly, A.M., Martini, A.M., Blake, R.E., 2004. Sites of anomalous organic remineralization in the carbonate sediments of South Florida, USA: the sulfur cycle and carbonate-associated sulfate. In: Amend, J., Edwards, K., Lyons, T. (Eds.), Sulfur Biogeochemistry—Past and Present: *Geological Society of America Special Paper* vol. 379, pp. 161–176.

Maric, M., Fralick, P.W., 2005. Sedimentology of the Rove and Virginia Formations and their tectonic significance. *Ins. Lake Super. Geol.* **51**, 41–42.

Morey, G.B., 1973. Stratigraphic framework of middle Proterozoic rocks in Minnesota. In: Young, G.M. (Ed.), Huronian Stratigraphy and Sedimentation. *Geological Association of Canada Special Paper* vol. 12, pp. 211–249.

Mojzsis, S.J., Coath, C.D., Greenwood, J.P., McKeegan, K.D., Harrison, T.M., 2003. Mass-independent isotope effects in Archean (2.5 to 3.8 Ga) sedimentary sulfides determined by ion microprobe analysis. *Geochim. Cosmochim. Acta* **67** (9), 1635–1658.

Neretin, L.N., Volkov, II, Bottcher, M.E., Grinenko, V.A., 2001. *A sulfur budget for the Black Sea anoxic zone.* Deep-Sea Research Part I-Oceanographic Research Papers, vol. 48 (12), pp. 2569–2593.

Ojakangas, R.W., 1983. Tidal deposits in the Early Proterozoic basin of the Lake Superior region—the palms and Pokegama Formations: evidence for subtidal-shelf deposition of superior-type banded iron-formation. In: Medaris, L.G. (Ed.), Early Proterozoic Geology of the Great Lakes Region, *Geological Society of America Memoir* vol. 160, pp. 49–66.

Ojakangas, R.W., Morey, G.B., Southwick, D.L., 2001. Palaeoproterozoic basin development and sedimentation in the Lake Superior region, North America. *Sediment. Geol.* **141**, 319–341.

Ono, S., Eigenbrode, J.L., Pavlov, A.A., Kharecha, P., Rumble, D., Kasting, J.F., Freeman, K.H., 2003. New Insights into the Archean sulfur cycle from mass-independent sulfur isotope records from the Hamersley Basin, Australia. *Geochim. Cosmochim. Acta* **6706**, 1–16.

Ono, S., Wing, B.A., Johnston, D.T., Farquhar, J., Rumble, D., 2006. Mass-dependent fractionation of quadruple stable sulfur isotope system as a new tracer of sulfur biogeochemical cycles. *Geochim. Cosmochim. Acta* **70**, 2238–2252.

Papineau, D., Mojzsis, S.J., Coath, C.D., Karhu, J.A., McKeegan, K.D., 2005. Multiple sulfur isotopes of sulfides from sediments in the aftermath of Paleoproterozoic glaciations. *Geochim. Cosmochim. Acta* **69** (21), 5033–5060.

Pavlov, A.A., Kasting, J.F., 2002. Mass-independent fractionation of sulfur isotopes in Archean sediments: strong evidence for an anoxic Archean atmosphere. *Astrobiology* **2** (1), 27–41.

Paytan, A., Kastner, M., Campbell, D., Thiemens, M.H., 1998. The sulfur isotopic composition of Cenozoic seawater sulfate. *Science* **282** (5393), 1459–1462.

Paytan, A., Kastner, M., Campbell, D., Thiemens, M.H., 2004. Seawater sulfate isotope fluctuation is the cretaceous. *Science* **304** (5677), 1663–1665.

Poulton, S.W., Fralick, P.W., Canfield, D.E., 2004. The transition to a sulphidic ocean ~1.84 billion years ago. *Nature* **431** (7005), 173–177.

Poulton, S.W., Canfield, D.E., 2005. Development of a sequential extraction procedure for iron: implications for iron partitioning in continentally derived particulates. *Chem. Geol.* **214** (3-4), 209–221.

Pufahl, P.K., Fralick, P.W., 1995. Paleogeographic reconstruction of the Gunflint–Mesabi–Cuyuna depositional system: a basin analysis approach. *Proc. Ins. Lake Super. Geol.* **41**, 59–60.

Pufahl, P.K., Fralick, P.W., 2004. Depositional controls on Paleoproterozoic iron formation accumulation, Gogebic Range, Lake Superior region, USA. *Sedimentology* **51**, 791–808.

Pufahl, P.K., Fralick, P.W., Scott, J., 2000. Depositional environments of the Palaeoproterozoic Gunflint Formation. In: Fralick, P.W. (Ed.), *Institute of Lake Superior Geology Field Guide* vol. 46, p. 46.

Rees, C.E., 1978. Sulphur isotope measurements using SO_2 and SF_6. *Geochim. Cosmochim. Acta* **42**, 383–389.

Rouxel, O.J., Bekker, A., Edwards, K.J., 2005. Iron isotope constraints on the Archean and Paleoproterozoic ocean redox state. *Science* **307** (5712), 1088–1091.

Shen, Y.N., Canfield, D.E., Knoll, A.H., 2002. Middle Proterozoic ocean chemistry: evidence from the McArthur Basin, northern Australia. *Am. J. Sci.* **302** (2), 81–109.

Shen, Y., Knoll, A.H., Walter, M.R., 2003. Evidence for low sulphate and anoxia in a mid-Proterozoic marine basin. *Nature* **423** (6940), 632–635.

Sims, P.K., Van Schmus, W.R., Schulz, K.J., Peterman, Z.E., 1989. Tectonostratigraphic evolution of the Early Proterozoic Wisconsin

magmatic terranes of the Penokean orogen. *Can. J. Earth Sci.* **26**, 2145–2158.

Sørensen, K.B., Canfield, D.E., 2004. Annual fluctuations in sulfur isotope fractionation in the water column of a euxinic marine basin. *Geochim. Cosmochim. Acta* **68** (3), 503–515.

Southwick, D.L., Morey, G.B., 1991. Tectonic imbrication and foredeep development in the Penokean Orogen, east-central Minnesota—an interpretation based on regional geophysics and the results of test-drilling. *United States Geological Survey Bulletin*, 1904-C, 17.

Strauss, H., 1993. The sulfur isotopic record of precambrian sulfates—new data and a critical-evaluation of the existing record. *Precambrian Res.* **63** (3-4), 225–246.

Strauss, H., 2004. 4 Ga of seawater evolution. In: Amend, J., Edwards, K., Lyons, T. (Eds.), *Sulfur Biogeochemistry—Past and Present*. Geological Society of America Special Paper, vol. 379, pp. 195–210.

Turchyn, A.V., Schrag, D.P., 2004. Oxygen isotope constraints on the sulfur cycle over the past 10 million years. *Science* **303** (5666), 2004–2007.

Van Wyck, N., Johnson, C.M., 1997. Common lead, Sm–Nd, and U–Pb constraints on petrogenesis, crustal architecture and tectonic setting of the Penokean Orogen (Paleoproterozoic) in Wisconsin, USA. *Geol. Soc. Am. Bull.* **109**, 799–808.

Walker, J.C.G., Bimblecombe, P., 1985. Iron and sulfur in the pre-biologic ocean. *Precambrian Res.* **28** (3-4), 205–222.

Wing, B.A., Lyons, J.R., Farquhar, J., 2004. Experimental constrinats on anomolous S-isotopic fracitonation during UV irradiation of SO_2. *Geochim. Cosmochim. Acta* **68** (11), A781.

Zmolek, P., Xu, X.P., Jackson, T., Thiemens, M.H., Trogler, W.C., 1999. Large mass independent sulfur isotope fractionations during the photopolymerization of (CS2)-C-12 and (CS2)-C-13. *J. Phys. Chem. A* **103** (15), 2477–2480.